Molecular Modeling Exercises and Experiments

edited by
Ronald Starkey
University of Wisconsin–Green Bay
Green Bay, WI 54311-7001

Integrating Molecular Modeling into the Inorganic Chemistry Laboratory

W

Craig D. Montgomery
Department of Chemistry, Trinity Western University, Langley, BC V2Y 1Y1, Canada; *montgome@twu.ca*

Molecular modeling has become a vital technique in chemical research, and while there are some unique challenges in the modeling of d- and f-block complexes (*1*), the realm of molecular modeling also includes inorganic chemistry (*2*). Molecular modeling is finding its way into the undergraduate chemistry curriculum, as well (*3*). In this paper, a variety of molecular modeling techniques are applied to four common inorganic chemistry experiments. Each of the lab experiments considered here is currently part of the lab component of an upper-level course in transition metal chemistry at my institution. For each experiment, a lab exercise in molecular modeling is presented to accompany rather than replace the experiment. The benefits of these exercises include

1. enhancing the students' understanding of the theoretical concepts presented by the lab experiment;
2. helping the students to visualize molecular structures and orbitals; and
3. giving the students an introduction to molecular modeling.

Comments from students have reflected these benefits.

The modeling software used in this work was *HyperChem* (*4*), but the exercises can be adapted to other software packages. I will provide step-by-step instructions for performing these exercises with *HyperChem* upon request.

Preparation of Lewis Acid–Base Complex

While this experiment does not involve transition metals, it is nevertheless a common experiment (*5*) in such courses for at least two reasons. It is a simple example of a coordinate bond as encountered in transition metal compounds and more importantly, it introduces the student to an important lab technique in transition metal chemistry, the use of a vacuum rack. $NMe_3(g)$ reacts with $BF_3(g)$ to form the white solid adduct whose stoichiometry can be determined (eq 1). IR spectroscopy is used to characterize the product. Anderson (*6*) describes an alternate modeling exercise for such Lewis acid–base reactions.

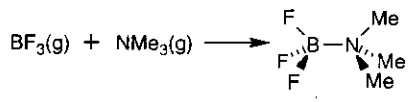

(1)

Purpose of Molecular Modeling Exercise

The purpose of this exercise is to determine the orbitals involved in the formation of the coordinate bond between BF_3 and NMe_3 and predict the effect of the formation of the B–N bond upon the B–F stretching frequency. The IR spectra of both BF_3 and the BF_3NMe_3 complex are then determined.

Procedure

1. Both the BF_3 and NMe_3 compounds are drawn and converted into three-dimensional structures using the "build" command.
2. The geometry of each compound is optimized using first molecular mechanics (MM+ force field) and then semiempirical methods (AM1).[1]
3. This semiempirical calculation of the optimized structures also yields a series of molecular orbitals that can be examined, including the BF_3 LUMO and the NMe_3 HOMO.
4. The vibrational spectrum of BF_3 is determined using ab initio methods (STO-3G basis set).
5. Steps 1, 2, and 4 are repeated for the F_3B–NMe_3 complex.

Results

Convergence to an optimized structure is obtained in each case. The charges on nitrogen and carbons in the optimized NMe_3 are −0.137 and +0.082, respectively; the charges on boron and fluorines in BF_3 are 0.731 and −0.224, respectively.

The molecular orbital energy level diagrams are consistent with other such diagrams for these compounds (*7*). The HOMO of NMe_3 is the $4A_1$ orbital[2] with an energy of −9.12 eV. There is evidence in the BF_3 molecular orbital diagram of π bonding. The LUMO of BF_3 is the $2A_2''$ orbital with an energy of 1.62 eV, and as can be seen from the edge-on view of Figure 1, it is a π*-type orbital; the $1A_2''$ orbital at −15.15 eV is the corresponding π_b orbital. Therefore when the B–N bond is formed upon donation of the electron pair into this orbital, one would expect a weakening of the B–F bond accompanied by a decrease in the B–F stretching frequency.

The shifting of the B–F vibrational frequencies can be examined further by considering the IR spectrum calculated

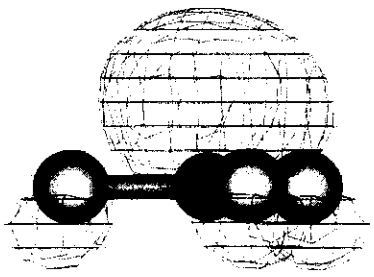

Figure 1. An edge-on view of the BF_3 π* LUMO.

Table 1. Calculated and Experimental Vibrational Frequencies for BF_3 and BF_3NMe_3

B–F Vibrational Mode	Vibrational Frequency/cm^{-1}			
	Calculated[a]		Literature	
	BF_3	BF_3NMe_3	BF_3 (8)	BF_3NMe_3 (9)
Deformation	521	499	482	340
Deformation	709	641	718	550
Symmetric stretch	990	976	888	952
Asymmetric stretch	1710	1634	1505	1165

[a]Calculated by ab initio methods using an STO-3G basis set.

for both BF_3 and the BF_3NMe_3 complex. The results of these calculations, along with the literature values, appear in Table 1. The most accurate values were obtained with ab initio methods; however, such calculations are time-consuming in the case of the BF_3NMe_3 complex. For faster results with less accuracy, AM1 semiempirical methods may be used. In the case of each of the four vibrational modes of BF_3, the calculated vibrational frequency decreases upon formation of the adduct as predicted based on consideration of the molecular orbitals.

A comparison with the literature values indicates that these predicted shifts are actually observed. Each of the BF_3 vibrational frequencies decreases on formation of the complex with the exception of the symmetric stretch (*8*, *9*). The anomalous behavior of the B–F symmetric stretch is due to mixing with the B–N stretching mode in the case of the complex to give out-of-phase and in-phase NBF_3 symmetric stretches (*9*).

Preparation of Linkage Isomers

Another common experiment in an undergraduate course in transition metal chemistry is the preparation of linkage isomers, specifically $[Co(NH_3)_5(NO_2)]Cl_2$ and $[Co(NH_3)_5(ONO)]Cl_3$ (eq 2).

$$[Co(NH_3)_5Cl]Cl_2 \xrightarrow[2.\ HCl\ \ 3.\ NaNO_2]{1.\ NH_3} [Co(NH_3)_5(ONO)]Cl_2 \xrightarrow{\Delta} [Co(NH_3)_5(NO_2)]Cl_2 \qquad (2)$$

Purpose of Molecular Modeling Exercise

The purpose of this exercise is to determine the relative stabilities of the two isomers and to determine a possible transition state.

Procedure

1. The two isomers are drawn and converted into a three-dimensional structure using the "build" command.

2. The geometries of the two structures are optimized first using molecular mechanics (MM+ force field) and then semiempirical quantum mechanical means (PM3, then ZINDO/1).[1]

3. The transition state is determined by the method of synchronous transit[3] with a PM3 calculation.[1]

Results

Convergence to an optimized geometry is obtained for both isomers. It should be noted that for each isomer, the arrangement of the ONO ligand plane in the optimized geometry depended on the choice of semiempirical method. The lowest energy conformations, which are described below, were obtained by the use of PM3 followed by ZINDO/1. Individuals doing this exercise might find it useful to repeat the geometry optimization using various semiempirical methods.

The optimized structure of the nitrito isomer is shown in Figure 2 with the hydrogen atoms omitted for clarity. The ONO plane is directed between cis NH_3 groups as indicated by an *N(cis)*–Co–O–N torsion angle of 44.0°. Also the Co–O–N–O torsion angle of -179.9° indicates that the Co is virtually coplanar with the NO_2 fragment. The Co–O bond length is 1.839 Å.

The optimized nitro structure is likewise shown in Figure 3. In this case the NO_2 ligand is directed in a fashion coplanar with an N–Co–N fragment as indicated by the H_3N–Co–N–O torsion angles of 0.3° and 1.0°. The Co–N bond distance is 1.961 Å.

The single-point energies for the nitro and nitrito structures are -3897.0 and -3885.6 kcal/mol, respectively, which allows the experimenter to correctly predict that the nitro isomer is thermodynamically preferred (by 11.4 kcal/mol).

Evidence such as interconversion occurring in the solid state, rapid interconversion rates in solution even in the absence of excess nitrate, and results of ^{18}O labeling experiments

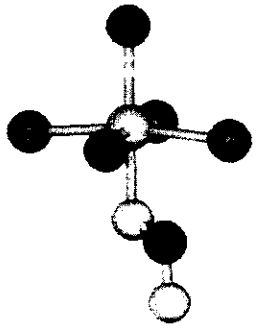

Figure 2. The optimized geometry of $[Co(NH_3)_5(ONO)]^{2+}$ (hydrogen atoms omitted for clarity).

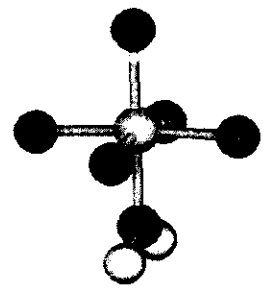

Figure 3. The optimized geometry of $[Co(NH_3)_5(NO_2)]^{2+}$ (hydrogen atoms omitted for clarity).

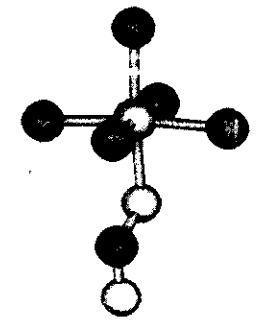

Figure 4. A possible transition state in the nitrito-to-nitro isomerization.

suggests that the mechanism of isomerization from nitrito to nitro is intramolecular, S_Ni (*10*). In this exercise, a possible transition state is found. It is one in which the nitrito ligand has rotated around the Co–O bond so that the ONO ligand is now positioned closer to the plane formed by the Co and two ammonia nitrogen atoms (H_3N–Co–O–N torsion angles of 12.4° and -167.8°), as seen in Figure 4. This transition state can then move toward the nitro isomer via an in-plane rotation of the NO_2 ligand; this sort of step has been proposed previously for such isomerizations on the basis of solid-state X-ray studies (*11*).

Preparation and Characterization of [1,3,5-CH_3(CH_3)]Mo(CO)$_3$

The three-legged piano stool complex, [1,3,5-CH_3(CH_3)]Mo(CO)$_3$ (*12*), is prepared by refluxing Mo(CO)$_6$ in mesitylene under nitrogen (eq 3). The product is characterized by NMR and IR spectroscopy, specifically considering the CO stretches in the latter.

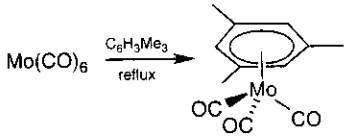

(3)

Purpose of the Molecular Modeling Exercise

It can be useful, as an exercise in the application of group theory, to have the students calculate the number of IR-active CO stretching modes and the number of IR bands to which they will give rise. While this can readily be done with a set of character tables, molecular modeling is used here to extend this exercise, allowing students to evaluate the energies of these stretching modes and to visualize the modes.

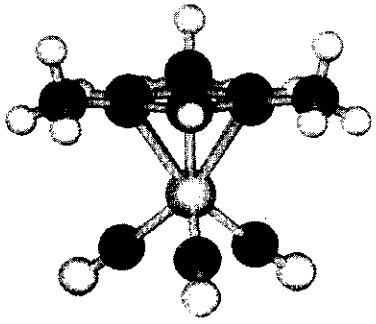

Figure 5. The optimized geometry of [1,3,5-CH_3(CH_3)]Mo(CO)$_3$.

Table 2. CO Stretching Frequencies for [1,3,5-C_6H_3(CH_3)$_3$]Mo(CO)$_3$

Vibrational Mode	Stretching Frequency/cm^{-1}	
	Calculated[a]	Experimental (*13*)
Asymmetric CO stretch (E)	1979	1904
Symmetric CO stretch (A)	2067	1976

[a]Calculated using PM3 semiempirical methods.

Procedure

1. Both mesitylene and Mo(CO)$_3$ are drawn and converted into three-dimensional structures.
2. The Mo(CO)$_3$ is then oriented approximately correctly with respect to the mesitylene and the six Mo–C(mesitylene) bonds are added.
3. The geometry of the structure is optimized first by molecular mechanics (MM+)[1] and then by semiempirical methods (PM3).[1]
4. The vibrational spectrum is calculated for the optimized geometry by semiempirical methods (PM3).[1]

Results

The geometry optimization calculation results in convergence to a three-legged piano stool structure of C_3 symmetry as shown in Figure 5. Bond lengths are as follows: Mo–C(Me) (2.430 Å), Mo–CH (2.387 Å), Mo–CO (1.946 Å), C–O (1.174 Å); the C(carbonyl)–Mo–C(carbonyl) and Mo–C–O bond angles are 87.8° and 177.1°, respectively. The methyl groups on the arene ring appear to be bent away from the Mo atom while the arene ring hydrogen atoms remain in the plane of the ring. The ring torsion angles confirm this; the C–C–C–CH_3 torsion angles are -170.5° and the C–C–C–H angles are 179.5°.

The results of the IR calculations are shown in Table 2.

Chromatography of Ferrocene Derivatives

In this experiment, a Friedel–Crafts acetylation of the cyclopentadienyl (Cp) ring of ferrocene is carried out (eq 4) and the products are separated by column chromatography before being characterized by IR and ^{1}H NMR spectroscopy (*14*).

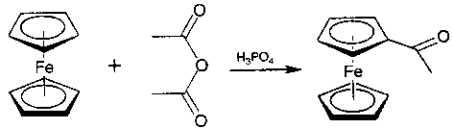

(4)

Purpose of Molecular Modeling Exercise

The purpose of the modeling exercise is to determine the energy barrier for ring rotation for ferrocene and the monosubstituted product. The analogous calculation is also done for decamethylferrocene, for purposes of comparison.

Procedure

1. An eclipsed ferrocene molecule is drawn and converted to a three-dimensional structure using the "build" command.
2. The geometry is optimized by molecular mechanics (MM+ force field).
3. The geometry is optimized again, this time by a semiempirical quantum mechanical method (PM3).[1]
4. One of the Cp rings is detached from the iron atom and rotated 36° to give a staggered conformation before being reattached to the iron atom. Step 3 is repeated.
5. A hydrogen atom on one ring of the eclipsed ferrocene structure is replaced by an acetyl group and step 3 is repeated. (In this case, it is necessary to restrain the H–C–Fe–C torsion angles between the rings so as to maintain the eclipsed conformation when optimizing the geometry. The restraints are then removed for a single-point calculation.)

6. A hydrogen atom on one ring of the staggered ferrocene structure is replaced by an acetyl group and step 3 is repeated. (In this case, it is again necessary to restrain the H–C–Fe–C torsion angles between the rings so as to maintain the staggered conformation when optimizing the geometry. The restraints are then removed for a single-point calculation.)

7. Step 5 may be repeated with no restraints applied in order to determine the most stable conformation.

8. Each of the hydrogen atoms on the eclipsed ferrocene structure is replaced by a methyl group and step 3 is repeated. (Again it is necessary to restrain the C–C–Fe–C torsion angles between the rings so as to maintain the eclipsed conformation when optimizing the geometry. The restraints are then removed for a single-point calculation.)

9. Each of the hydrogen atoms on the staggered ferrocene structure is replaced by a methyl group and step 3 is repeated.

Results

Both of the conformations of ferrocene converge to an optimized structure with Fe–C bond distances of 2.085 and 2.087 Å for the eclipsed and staggered geometries, respectively, compared with experimental values of 2.064 Å (*15*). The single-point energies calculated are -2496.3 and -2495.7 kcal for the eclipsed and staggered conformations respectively, indicating that the eclipsed conformation is actually favored by 0.6 kcal/mol. While it should be noted that such an energy difference may be too small to be considered reliable, nevertheless this result is consistent with previous results (*15*). These earlier studies showed that the staggered and eclipsed conformations of ferrocene are indeed very close in energy, the eclipsed structure being preferred. (Whereas in the solid state, crystal packing factors result in the staggered conformation being favored.)

When one acetyl group is added to ferrocene giving $Fe(CH_3C(O)Cp)(Cp)$, the energy barrier increases slightly as expected, becoming 1.0 kcal/mol, again in favor of the staggered structure. However, when the geometry is optimized with no restraints applied, an intermediate conformation (with H–C–Fe–C torsion angles ranging from 7.6° to 13.8°) is obtained as the optimum structure. This optimum conformation is illustrated in Figure 6. The oxygen atom is directed toward the other Cp ring, whereas the methyl group is directed away from the other ring.

In the case of decamethylferrocene, the energy difference has been determined to be about 2 kcal/mol (*10*) and the staggered conformation is more stable. In this study, the staggered form of decamethylferrocene is favored by 6.1 kcal/mol. In addition, the methyl groups are bent away slightly from the iron atom, which is also consistent with previous studies (*15*).

The results of the energy calculations in this study are summarized in Table 3.

Conclusions

The exercises described in this paper illustrate how molecular modeling can readily be used to enhance students' understanding of lab experiments in inorganic chemistry. Through molecular modeling, students are better able to visualize three-dimensional structures, determine and examine molecular orbitals, compare stabilities of isomers and conformers, determine possible transition states, and calculate spectroscopic properties.

Supplemental Material

Supplemental material for this article is available in this issue of *JCE Online*.

Notes

1. Geometry optimizations for semiempirical and molecular mechanics calculations both had a termination condition of less than 0.1 kcal/(Å mol) (decreased to 0.01 before vibrational spectrum calculations) with a Polak–Ribiere algorithm. The setup for semiempirical calculations typically involved a convergence limit of 0.01 kcal/mol, RHF spin pairing, and accelerated convergence.

2. The orbital notation denotes (by the first number) the relative energy and the symmetry of the orbital. For example, the notation $4A_1$ indicates that this orbital is the fourth lowest energy orbital and that it is of A_1 symmetry.

3. In the synchronous transit method, each atom in the reactant molecule (nitrito isomer) is matched up with an atom in the product molecule (nitro isomer). The starting point for the transition-state search is interpolated approximately midway between the reactant and product configurations. A vibrational calculation is done, a vibrational eigenvector is chosen, and then the search proceeds along that vibrational mode. Here transition-state searches were done by synchronous transit with quadratic interpolation and a termination condition of less than 0.1 kcal/(Å mol).

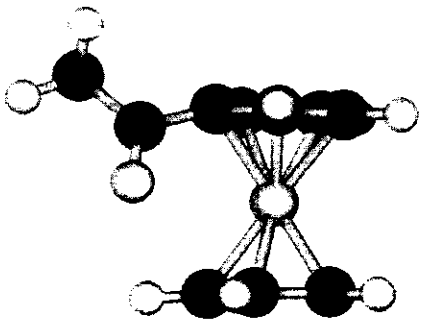

Figure 6. The optimized geometry of $Fe(CH_3C(O)Cp)(Cp)$.

Table 3. Calculated Energies of Staggered and Eclipsed Conformations of Ferrocene and Ferrocene Derivatives

Compound	Energy/(kcal mol^{-1})			Favored Configuration
	Conformation		Difference	
	Eclipsed	Staggered		
Ferrocene, $Fe(Cp)_2$	-2496.3	-2495.7	0.6	eclipsed
Acetyl compound $Fe(acetylCp)(Cp)$	-3049.1	-3050.1	1.0	staggered[a]
Decamethylferrocene $Fe(Cp^*)_2$	-5366.0	-5372.1	6.1	staggered

NOTE: Calculated in this study using PM3 semiempirical methods.
[a]See explanation in text.

Literature Cited

1. Cundari, T. R. *J. Chem. Soc., Dalton Trans.* **1998**, 2771–2776.
2. Comba, P., Hambley, T. W. *Molecular Modeling of Inorganic Compounds*; VCH: New York, 1995.
3. Pfennig, B. W.; Frock, R. L. *J. Chem. Educ.* **1999**, *76*, 1018–1022. Gasyna, Z. L.; Rice, S. A. *J. Chem. Educ.* **1999**, *76*, 1023–1029. Martin, N. H. *J. Chem. Educ.* **1998**, *75*, 241–243. Comba, P.; Zimmer, M. *J. Chem. Educ.* **1996**, *73*, 108–110.
4. *HyperChem Professional*, version 5.1; Hypercube, Inc: Gainesville, FL, 1998.
5. Angelici, R. J. *Synthesis and Technique in Inorganic Chemistry;* Saunders: Philadelphia, 1977; pp 198–205.
6. Anderson, P. F. *J. Chem. Educ.* **2000**, *77*, 209–215.
7. Miessler, G. L.; Tarr, D. A. *Inorganic Chemistry*, 2nd ed.; Prentice-Hall: Upper Saddle River, NJ, 1998; p 145.
8. Vanderryn, J. *J. Chem. Phys.* **1959**, *30*, 331. Dows, D. A. *J. Chem. Phys.* **1959**, *31*, 1637.
9. Amster, R. A.; Taylor, R. C. *Spectrochim. Acta* **1964**, *20*, 1487–1502.
10. Basolo, F.; Pearson, R. G. *Mechanisms of Inorganic Reactions*, 2nd ed.; Wiley: New York, 1967; pp 291–294.
11. Grenthe, I.; Nordin, E. *Inorg. Chem.* **1979**, *18*, 1109.
12. Angelici, R. J. *Synthesis and Technique in Inorganic Chemistry;* Saunders: Philadelphia, 1977; pp 129–146.
13. Fischer, E. O.; Oefele, K.; Essler, H.; Frohlich, W.; Mortensen, J. P.; Semmlinger, W. *Chem. Ber.* **1958**, *91*, 2763.
14. Angelici, R. J. *Synthesis and Technique in Inorganic Chemistry;* Saunders: Philadelphia, 1977; pp 157–168.
15. Lukehart, C. M. *Fundamental Transition Metal Organometallic Chemistry*; Brooks/Cole: Monterey, CA, 1985; p 90.

Molecular Modeling Exercises and Experiments

Mechanisms of Pentacoordinate Pseudorotation. A Molecular Modeling Study of PF_5

W

Craig D. Montgomery

Department of Chemistry, Trinity Western University, Langley, BC V2Y 1Y1, Canada; *montgome@twu.ca*

Pentacoordinate phosphorus compounds or phosphoranes are, with few exceptions, trigonal bipyramidal (TBP) in geometry; the exceptions are monocyclic and bicyclic phosphoranes, where ring strain is a factor (*1*). However, one of the unique properties exhibited by some pentacoordinate compounds that is commonly noted in inorganic chemistry courses and texts is that of pseudorotation, whereby axial and equatorial substituents of the trigonal bipyramid exchange sites without breaking any bonds. Evidence for such pseudorotation comes most often from NMR spectroscopy. A well-known example is PF_5, which exhibits one signal, a doublet, in the ^{19}F NMR above -22 °C (*2*).

Two mechanisms appear possible for the pseudorotation process—the Berry process and the turnstile process, illustrated in Schemes I and II, respectively. In the Berry mechanism, the axial angle (∠DPE in Scheme I) of 180° closes down to 150° at the same time as one of the equatorial bond angles ∠BPC in Scheme I) opens up to 150°; this brings the molecule to the square pyramidal (SP) transition state in the mechanism. Angle DPE then continues to close down until reaching 120°, at which point substituents D and E are in the equatorial positions. Likewise, ∠BPC simultaneously continues to open up until it reaches 180°, at which point B and C have become axial substituents.

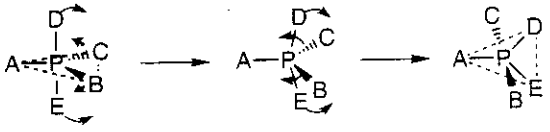

Scheme I: Berry pseudorotation mechanism

In the alternate mechanism, a pair of substituents (A and D in Scheme II), rotates with respect to the remaining three substituents in the manner of a turnstile. (In Scheme II, B rotates toward C, C toward E, and E toward B.) Before this rotation takes place the structure must distort slightly in order to align itself with the turnstile axis; after the rotation it distorts back to a TBP structure. The transition state in the turnstile mechanism is the 30° TR structure and it lies midway through the rotation step; that is, B has rotated halfway toward the position of C, etc.

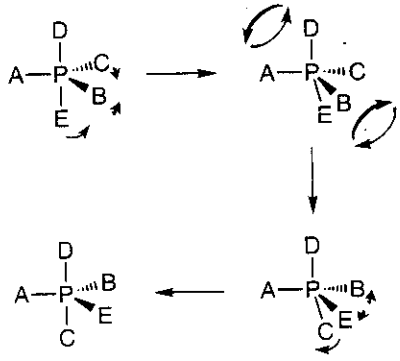

Scheme II: turnstile pseudorotation mechanism

Both of these transition states (SP, 30° TR) are illustrated in Scheme III. Holmes et al. (*3*) have argued in favor of the Berry mechanism on the basis of solid-state structural distortions, although some turnstile-type distortions have also been noted (*4*).